

Statistically reconstructing continuous isotropic and anisotropic two-phase media while preserving macroscopic material properties

M. A. Davis,^{*} S. D. C. Walsh, and M. O. Saar

Department of Geology and Geophysics, University of Minnesota, Twin Cities, Minnesota 55455, USA
(Received 2 September 2010; revised manuscript received 13 October 2010; published 28 February 2011)

We propose a method to generate statistically similar reconstructions of two-phase media. As with previous work, we initially characterize the microstructure of the material using two-point correlation functions (a subset of spatial correlation functions) and then generate numerical reconstructions using a simulated annealing method that preserves the geometric relationships of the material's phase of interest. However, in contrast to earlier contributions that consider reconstructions composed of discrete arrays of pixels or voxels alone, we generate reconstructions based on assemblies of continuous, three-dimensional, interpenetrating objects. The result is a continuum description of the material microstructure (as opposed to a discretized or pixelated description), capable of efficiently representing large disparities in scale. Different reconstruction methods are considered based on distinct combinations of two-point correlation functions of varying degrees of complexity. The quality of the reconstruction methods are evaluated by comparing the total pore fraction, specific surface area of the percolating cluster, pore fraction of the percolating cluster, tortuosity, and permeability of the reconstructions to those of a set of reference assemblies. Elsewhere it has been proposed that two-phase media could be statistically reproduced with only two spatial correlation functions: the two-point probability function (the probability that two points lie within the same phase) and the lineal path function (the probability that a line between two points lies entirely within the same phase). We find that methods employing the two-point probability function and lineal path function are improved if the percolating cluster volume is also considered in the reconstruction. However, to reproduce more complicated geometric assemblies, we find it necessary to employ the two-point probability, two-point cluster, and lineal path function in addition to the percolating cluster volume to produce a generally accurate statistical reconstruction.

DOI: [10.1103/PhysRevE.83.026706](https://doi.org/10.1103/PhysRevE.83.026706)

PACS number(s): 02.60.Pn, 91.60.Np, 83.80.Nb, 81.05.Rm

I. INTRODUCTION

Composite materials consisting of multiple phases (solids, voids, fluids) are prevalent in nature and synthetic products. Examples include soils [1], magma [2], blood [3,4], concrete [5], foams [6,7], and particulate composites [8,9]. In these media, the phases are composed of microstructures that determine large-scale, or macroscopic, material properties, such as bulk modulus, compressibility, viscosity, yield stress, electrical conductivity, and permeability [10], which dictate a system's behavior. Therefore, an improved understanding of how a composite material's microstructure affects its macroscopic properties has implications in numerous fields of science and engineering.

The relationship between microstructural features of composite materials and their macroscopic material properties has been investigated by several authors using two-point correlation functions (TPCFs) in combination with simulated annealing techniques [11–14]. First, the TPCFs (a subset of spatial correlation functions) are used to characterize certain geometric relationships of the material microstructure. Then, the simulated annealing algorithm is used to generate statistically similar reconstructions that preserve the same geometric microstructural relationships. A successful reconstruction occurs when the reference and reconstructed assemblies' spatial relationships match, while preserving the reference assembly's physical properties. Once an accurate

reconstruction is produced, the spatial relationships of that assembly's microstructure may be used to (i) gain a deeper understanding of how microstructure of a composite material affects macroscopic physical properties, improving our ability to modify these properties [10], and (ii) recreate the material in a larger quantity or different size while preserving material properties, even when the original construction process is unknown.

The reconstruction method proposed in this article differs from that in previous work in that it employs reference and reconstructed assemblies consisting of interpenetrating inclusions of continuous, geometric objects (Sec. III) rather than discretized objects represented by voxels (three-dimensional pixels). As a result, none of the reconstructions are performed on voxelized data, nor are voxelized assemblies created during the reconstruction process, which has been commonly employed (e.g., Refs. [10,13]). However, our method may also be used to reconstruct continuous objects from voxelized data as briefly discussed in Sec. II.

In prior work conducted on voxelized assemblies, Torquato and Stell [11] found the two-point probability function, $S(r)$, a type of two-point correlation function, alone to be insufficient in capturing the spatial microstructure characteristics of a homogeneous, isotropic assembly. Later, Yeong and Torquato [12,15] suggested that using $S(r)$ and the lineal path function, $S^l(r)$, together should be sufficient to accurately reconstruct a given isotropic (voxelized) assembly. In this contribution, different combinations of two-point correlation functions are considered to determine the most accurate and appropriate reconstruction method for continuous isotropic

^{*}davis923@umn.edu

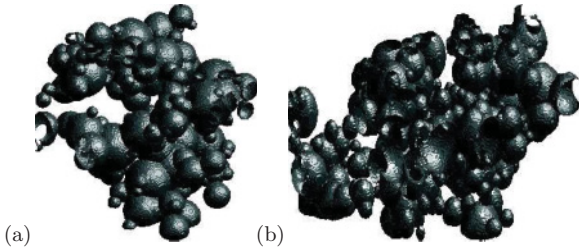


FIG. 1. Example of (a) isotropic spheroidal and (b) anisotropic ellipsoidal reference percolating phase of interest.

and anisotropic assemblies, as well as the effect of enriching the reconstruction method with additional information (e.g., the percolating cluster volume, calculated in the Appendix).

While results from this approach are generally applicable to a wide range of composite materials and macroscopic material properties, this study focuses on the problem of reconstructing porous media while preserving macroscopic permeability and tortuosity. An example of synthetic porous media is shown in Fig. 1. Permeability is chosen as the primary material property of interest because it is arguably the most important property in porous media fluid flow studies, as it largely determines fluid flow rates in such systems (e.g., Ref. [16]). We are particularly interested in how microstructure affects the permeability of porous media, as such insights form the basis for our magma permeability studies (e.g., Ref. [17]). In addition, permeability serves as an excellent macroscopic property test for any material reconstruction study, as it depends on multiple microstructure properties such as pore fraction and connectivity, specific surface area, and pore-space tortuosity. Permeability can also be determined for two-dimensional and three-dimensional images and can even be used to test two solid-phase reconstructions. Furthermore, permeability is directly related to electrical conductivity [18,19]. Therefore, referencing permeability provides a reconstruction measure for a wider variety of materials other than porous media.

Nonetheless, reproducing permeability is a necessary, but insufficient, condition to achieve an accurate reconstruction, as it is nonunique with respect to phase microstructure. For example, a thin straight tube could have the same permeability as a wider, but more tortuous, helix. Thus, two systems with identical permeabilities, but different microstructures, will exhibit a difference in other material properties, such as the specific surface area or path tortuosity. Therefore, in addition to permeability, our reconstruction method aims to preserve other macroscopic material properties such as phase volume fraction, specific surface area between phases, phase tortuosity, and the volume of space-spanning phase networks.

In Sec. II, we detail the methods (two-point correlation functions and simulated annealing) used to perform the assembly reconstructions. Section III discusses the types of assemblies used in this study and describes how physical characteristics are calculated and used to compare the reconstruction methods presented in this article. Finally, we discuss the results of the individual reconstruction methods in Sec. IV and conclude in Sec. V with reconstruction method recommendations that optimize reconstruction effectiveness and computational simplicity for isotropic and anisotropic assemblies.

II. RECONSTRUCTION METHOD

In this section, we describe the methods employed to statistically reconstruct composite materials. Our reference volumes are randomly generated assemblies of interpenetrating spheres and ellipsoids (Sec. III) to ensure all spatial properties of the original assembly are known. Each reference assembly is constructed by combining the TPCFs (Sec. II A) of 10 randomly produced assemblies for each of the assembly types (Sec. III). Our general reconstruction method proceeds as follows: (i) the spatial relationships of the reference and reconstructed assemblies are quantified using TPCFs and the percolating cluster volume (PCV) (Sec. III B), (ii) an initial assembly of spheroids is reconstructed with the same volume fraction and specific surface area as the reference assembly, and (iii) the simulated annealing algorithm (Sec. II B) is used to generate reconstructed assemblies by matching the reference and reconstructed assembly's TPCFs. The same functions may be employed to reconstruct natural samples, as long as two-dimensional or three-dimensional information exists for the medium of interest. This information may be collected in a variety of forms, such as voxelized images from serial cross sections or x-ray tomography imaging. In some cases, continuous, geometrically defined objects (e.g., spheres, ellipsoids, cuboids) may be provided whose parameters (radii, side lengths) are known. In such cases, geometric information may be determined using known generation mechanisms for the given assembly, such as chemical reactions, exsolution mechanisms, numerical generation, or biological formation.

In the simulated annealing algorithm used in our reconstruction process, the misfit between the functions (e.g., TPCFs or PCV) is minimized by modifying physical characteristics in the reconstructions. Our reconstruction method differs from other existing methods that are restricted to voxel-to-voxel reconstructions in that our method allows both voxelized and continuous object assemblies to be reconstructed. Thus, the proposed approach provides a means to transfer three-dimensional voxelized images to equivalent three-dimensional continuous object assemblies. This can be useful when inclusions, with some known characteristics (e.g., spheres or cuboids in a suspension or ellipsoids in foams and solidified magma), are reconstructed from voxelized x-ray tomography data. However, reconstructing a voxelized image as a continuous image (or vice versa) should be approached with caution, as resolution issues due to discretization, particularly of curved surfaces, may cause inaccurate representations of the medium in the resulting image, altering its physical material properties. Further discussion of this issue may be addressed in future publications.

In this contribution, discretized versions of the reconstructed assemblies are created to measure permeability (using lattice-Boltzmann simulations) and tortuosity (using a random-walker algorithm). The resolution of the discretized versions is set to $208 \times 208 \times 208$ voxels, chosen based on computational limitations at the time of processing. In general, the discrete resolution of a sample can impact the calculated numerical permeability or tortuosity, if the resolution is too low to capture the sample's microstructure. However, here we seek to compare measured permeabilities and tortuosities between samples rather than physical values. As the discretization is

consistent across all assemblies, the resulting permeability will be comparable, and any resolution lost in the discretization process is inconsequential.

A. Two-point correlation functions and the percolating cluster volume

This section describes the attributes of the three two-point correlation functions used in this study—a more detailed description of how the individual functions are calculated is provided in the Appendix.

The three two-point correlation functions employed are (i) the two-point probability or spatial autocorrelation function, (ii) the two-point cluster function, and (iii) the lineal path function. All three functions are related (Fig. 2). Given two random points separated by a distance, r , the three correlation functions are defined as follows: (i) the two-point probability function, $S(r)$, describes the probability that both points lie within the same phase of an assembly; (ii) the two-point cluster function, $S^c(r)$, describes the probability that the points can be joined by a nonlinear path contained within the same phase of an assembly; and (iii) the lineal-path function, $S^l(r)$, describes the probability that a line connecting two points is contained entirely within the same phase.

The three functions contain information about different aspects of an assembly. The two-point correlation function is sensitive to the spatial distribution of a given phase. The two-point cluster function is dependent on the distribution

and connectivity of the discrete components of that phase. The lineal path function describes the tortuosity of those components.

Several specific pieces of information about assembly microstructure can be gleaned directly from all three two-point correlation functions. For example, the pore fraction, ϕ , of the assembly is given by the y-axis intercept for the TPCFs, i.e.,

$$S(0) = S^c(0) = S^l(0) = \phi, \quad (1)$$

and the slope of all three functions as $r \rightarrow 0$, is proportional to the specific surface area, s , of the inclusions within the assembly:

$$s = -4 \left. \frac{\partial S(r)}{\partial r} \right|_{r=0} \quad (2)$$

for three-dimensional assemblies (the constant of proportionality differs depending on the number of dimensions) [20]. More information regarding the characteristics of these functions and their relationships to specific aspects of assembly microstructure is described in Refs. [10–12,14,15,21].

For isotropic, ergodic (statistically spatially invariant) assemblies, the different correlation functions are independent of orientation. However, this is not true for anisotropic materials, where the two-point correlation functions change depending on the orientation of the line segments connecting the two points. Accordingly, when examining anisotropic assemblies, we calculate two-point correlation functions along three orthogonal axes aligned with the principle directions of anisotropy. These two-point correlation functions are calculated in much the same manner as those given above, except the relative orientations of the two points are fixed instead of being random.

In isolation, the individual two-point correlation functions do not contain sufficient information to accurately describe an assembly's structure. However, increasingly accurate reconstructions can be obtained by combining two or more two-point correlation functions [12,15].

The following section describes a simulated annealing method that reconstructs an assembly of continuous, individual inclusions of arbitrary dimensions, orientations, and distributions rather than a voxelized image. This approach works best if the simulated annealing method is provided with an initial reconstruction that is, in a sense, close to the reference assembly being reconstructed. For isotropic assemblies, we select an initial configuration that contains randomly distributed equal-sized spheres with the same pore fraction and specific surface area as the reference assembly. The reference assembly's pore fraction and specific surface area can be determined from the two-point correlation functions for the reference assembly using Eqs. (1) and (2). The radius, R , and number density, n , of the spheres in the initial reconstruction are

$$R = -3(1 - \phi) \log(1 - \phi)/s; \quad (3)$$

$$n = -3 \log(1 - \phi)/(4.0\pi R^3). \quad (4)$$

These relationships are derived from the relationship between the volume fraction of an assembly of interpenetrating objects, ϕ , the number density, n , and volume, V , of each object,

$$\phi = \exp(-nV). \quad (5)$$

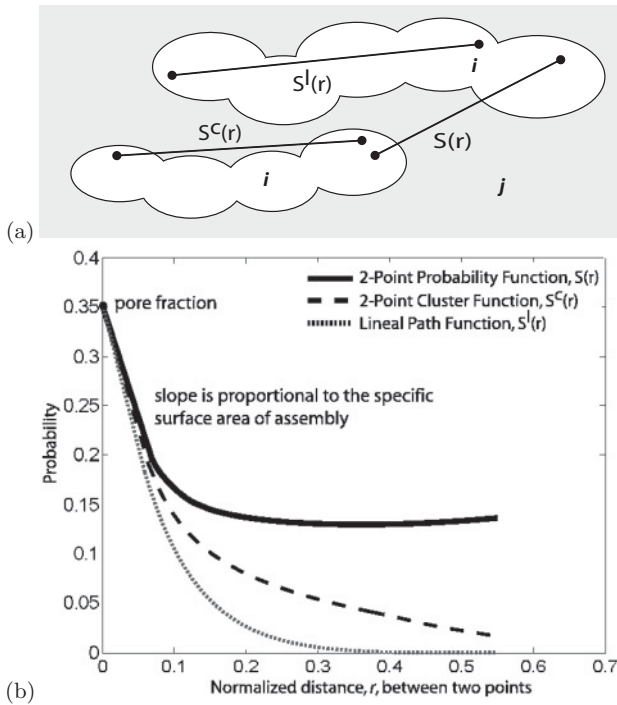


FIG. 2. (a) Two-dimensional illustration of two-point correlation functions (defined in the main text) used to statistically reconstruct the spatial relationships of inclusions of phase i within another phase j . (b) An example of a probability plot for the three TPCFs as a function of the distance between two points, r . The y intercept is equivalent to the pore fraction of the assembly and the slope at $r \rightarrow 0$ is proportional to the specific surface area.

While Eqs. (3) and (4) are specific to assemblies of spheres, equivalent expressions can be equally easily derived for isotropic assemblies of other inclusion shapes (e.g., cuboids; Ref. [17]).

For anisotropic media (e.g., continuous ellipsoids with preferred orientations), the initial reconstruction is a set of randomly distributed, equal-sized ellipsoids with aligned axes. In this case, we define three volume fractions, ϕ_x , ϕ_y , and ϕ_z , as well as three directional “surface areas,” s_x , s_y , and s_z , which correspond to the values obtained from the different two-point correlation functions with sample points aligned along the principle directions of anisotropy. Although, in theory, all three volume fractions should be identical, in practice, slight differences exist due to sampling error. Accordingly, the reference volume fraction is estimated by the mean pore fraction,

$$\phi = (\phi_x + \phi_y + \phi_z)/3. \quad (6)$$

In contrast, the directional surface areas need not be equal in anisotropic assemblies. The ratio between the three axes is a product of the degree of anisotropy of the component inclusion, and their relative alignment. By carefully selecting the particle number density, and the ellipsoidal radii of the inclusions, R_x , R_y , and R_z , an initial reconstruction is generated with the same volume fraction and directional surface area as the reference assembly. First, one of the directional surface areas is selected (say, s_x), then

$$R_x = -3(1 - \phi) \log(1 - \phi)/s_x, \quad (7)$$

$$n' = -3 \log(1 - \phi)/(4.0\pi R_x^3), \quad (8)$$

are found, where the variable R_x represents the ellipsoid radius in the x direction, while n' represents the number density necessary to construct an assembly of interpenetrating spheres with radii R_x with the same pore fraction as the reference assembly. The desired number density for the reconstructed assembly, n , is then given by rescaling n' as

$$n = n' s_y s_z / s_x^2 \quad (9)$$

and the remaining ellipsoid radii are

$$R_y = R_x s_x / s_y, \quad (10)$$

$$R_z = R_x s_x / s_z. \quad (11)$$

In addition to TPCFs, we propose to include the PCV to provide additional spatial information of the phase topology for the reference and reconstructed assemblies during the reconstruction processes (Sec. IIB). The PCV is used as a fitting parameter to match the volume fraction of percolating clusters in reference and reconstructed assemblies. In cases when the PCV is not used during the simulated annealing reconstruction process, it is used as an independent test of the reconstruction as discussed in Sec. IIIB.

B. Simulated annealing

Simulated annealing is employed to statistically reconstruct the reference assemblies based on the information contained in the TPCFs [10,22] and, in some cases, the newly introduced PCV. This is achieved by reducing the misfit between the

reference and the reconstructed assemblies for each of the functions' values.

Simulated annealing minimizes the misfit between the reference and reconstructed assemblies through a process of selective perturbation. First, perturbations are made to the initial reconstructed assembly. These perturbations affect the locations, orientations, volumes, and shapes (i.e., relative lengths of the ellipsoidal axes) of the individual inclusions, as opposed to altering a pixel or voxel phase type as typically performed on discretized assemblies (Ref. [12]). The goal of these perturbations is to reconstruct an assembly that more closely resembles the reference assembly. Each time a perturbation is made, the reconstruction's TPCFs, and, if employed, the PCV, are recalculated as described in Sec. II. The misfit between the reference and reconstructed assembly (referred to as the system energy, E) is then calculated from

$$E = \sum_{\alpha} \int_0^{r_{\max}} [S_{\text{ref}}^{\alpha}(r) - S_{\text{recon}}^{\alpha}(r)]^2 dr, \quad (12)$$

where S^{α} denotes the different two-point correlation functions employed in the reconstruction, chosen from the two point probability function, $S(r)$, the two-point cluster function, $S^c(r)$, the lineal path function, $S^l(r)$, and when applicable, the percolating cluster volume, PCV. The different combinations of two point correlation functions employed in this article are further discussed in Sec. III. The subscript ref denotes the reference assembly and recon indicates the reconstructed assembly. The perturbation is accepted unconditionally if it results in a reduction in E . Occasional unproductive perturbations are required to prevent the reconstructed assembly from resting in local minima. Thus, perturbations resulting in larger misfits between the reference and reconstructed assembly are accepted with a probability of

$$P(E) = \exp\left(-\frac{\Delta E}{\beta}\right), \quad (13)$$

where ΔE is the change in energy as a result of the perturbation and β is a scaling factor controlling the rate at which unproductive perturbations are accepted. Over the course of the simulated annealing process, β is decreased in a sawtooth pattern: β is initially set to its maximum value, and at each time step is decreased by 1/1000. Once β is less than 1/36 of the previous maximum, it is increased by a factor of 9 and a new local maximum is recorded. In practice, the global minimum is typically unattainable in a finite number of perturbations. Instead, the simulated annealing process is stopped once a sufficiently accurate fit is achieved. Therefore, this process continues until a predetermined minimum energy is reached. Other cooling schedules, such as linear or exponential methods, have also been employed in reconstruction studies using voxelized assemblies [23]. However, these schedules have a higher probability of causing trapping in local minima (e.g., Ref. [23]).

III. METHOD EVALUATION USING PHYSICAL CHARACTERISTICS

Our primary interest is to reconstruct porous media, such as pumice clasts. Hence, we investigate synthetic assemblies constructed of spheroids and biaxial, prolate ellipsoids that are

randomly distributed within a unit box (Fig. 1). The inclusion volumes are formed by discrete, interpenetrating objects that are normalized to the unit box and exhibit a log-normal volume distribution in the reference assemblies. The log-normal volume distribution loosely replicates the power-law bubble volume distribution found in some volcanic pumice samples [24]. In our reference assemblies, each inclusion volume is between 0.01% and 1.00% of the unit box volume. In this article, we explore three ergodic, synthetic reference assemblies: an isotropic assembly of spherical inclusions, an isotropic assembly of randomly oriented ellipsoids, and an anisotropic assembly of preferentially oriented ellipsoids. Other volume distributions could also be applied to our reconstruction method but are not expected to change the results for assembly reconstructions.

The reconstruction methods we are testing employ combinations of three TPCFs $S(r)$, $S^l(r)$, and $S^c(r)$ as well as the PCV. The sets of functions (Sec. II A) used in the simulated annealing process (Sec. II B) to reconstruct the three synthetic assembly types are given in Table I. Methods 6a, 6b, and 6c are of particular interest for reconstructing anisotropic assemblies.

To obtain inclusion information in each of the plane orientations, we project all inclusions in turn onto the xy , yz , and xz planes of the cubic coordinate system. For isotropic assemblies we use the method employed in Ref. [15], where the TPCFs are averaged over all three sampled directions (Methods 1–6a, excluding 4b), resulting in single correlation functions for $S(r)$, $S^c(r)$, and $S^l(r)$. Using this method may produce artificial anisotropy in the reconstruction, particularly in systems with long-range correlations, as discussed in Refs. [25,26]. This is not the case in the present article, as the target assemblies are created from ergodic assemblies of freely overlapping objects. Nevertheless, systems with long-range correlations may be reconstructed by introducing a sampling regime that encompasses all possible directions (to eliminate the artificial anisotropy) using the methods discussed in the Appendix. For anisotropic assemblies, we complete reconstructions using both the projected and averaged TPCFs (Method 6c) as well as reconstructions using only the projected TPCFs (Methods 4b and 6b). Each of the reconstruction methods are evaluated

based on their ability to preserve the reference assembly's microstructure and macroscopic material properties.

Reconstruction Methods 1–3 are motivated by combinations of TPCFs employed in previous studies [10–12,14,15]. Methods 4–6 are an extension of the work conducted by the previously mentioned authors in an attempt to develop a reconstruction method that better captures the topology and related material properties of anisotropic assemblies. Furthermore, Jiao *et al.* [27] found that when a clustering function is included in their reconstruction process, the resulting microstructure better preserves inclusion connectedness and the assembly's overall (discretized) texture. Preserving inclusion connectedness at the microscopic scale is imperative to investigating other physical properties at the macroscopic scale. Therefore, we use a clustering function in Methods 4–6 [PCV or $S^c(r)$] to better capture the percolating pathways in a given assembly. We are also interested in determining if Methods 1–3 are capable of statistically reproducing anisotropic assemblies while preserving said topology.

For each method presented in Sec. III, 10 reconstructions are performed. We chose to reconstruct 10 assemblies for each method to balance a reasonable sample size with computational cost. Further, these reconstructions are based on a single composite reference assembly for each assembly type (isotropic spheroids/ellipsoids, anisotropic ellipsoids). This composite reference assembly is the combination of 10 instances of reference assemblies, randomly created to produce a specific assembly type. The composite reference assembly is generated by averaging the TPCFs from all 10 assembly instances.

There are various validation parameters that can be implemented to determine the accuracy of a reconstruction. First, it is important to evaluate the goodness of fit between the reference and reconstructed assemblies' TPCFs (Table II). If the TPCFs do not exhibit a good fit, the simulated annealing process has likely been terminated prematurely. However, a good fit between the TPCFs of the reference and reconstructed assemblies does not necessarily indicate an accurate reconstruction of the microstructure topology and related macroscopic material properties have been produced. Therefore, determining the accuracy of a reconstruction requires some quantitative comparison to confirm that the reconstruction has statistically preserved the spatial relationships and macroscopic properties of the reference assembly. To provide a true independent assessment of the accuracy of a reconstruction, the macroscopic material properties being evaluated need to be independent of the reconstruction method employed (here, using Methods 1–6 in combination with simulated annealing). Thus, the validation parameters implemented here include the phase tortuosity (Sec. III A), percolating cluster volume, where applicable (Sec. III B), and permeability (Sec. III C). As the PCV is used in Methods 4a, 4b and 6a–6c during reconstructions, it cannot serve as an independent validation parameter for those methods. However, all of the physical characteristics should be examined when reviewing the success of a reconstruction method, including the pore fraction, ϕ , specific surface area of the percolating cluster, s_{PCV} , and the pore fraction of the percolating cluster, ϕ_{PCV} . By comparing all of the physical characteristics of the reference assembly to those of the reconstructed assembly, we can determine if

TABLE I. Sets of functions used for each reconstruction method in combination with simulated annealing. Isotropic spheroids and ellipsoids are reconstructed using Methods 1, 2, 3, 4a, 5, and 6a. Anisotropic ellipsoids are reconstructed using all methods shown below.

Method	Sets of functions used in reconstructions
1	$S(r)_{\text{avg}}$
2	$S^l(r)_{\text{avg}}$
3	$S(r)_{\text{avg}}, S^l(r)_{\text{avg}}$
4a	$S(r)_{\text{avg}}, S^l(r)_{\text{avg}}, \text{PCV}$
4b	$S(r)_{\text{proj}}, S^l(r)_{\text{proj}}, \text{PCV}$
5	$S(r)_{\text{avg}}, S^c(r)_{\text{avg}}, S^l(r)_{\text{avg}}$
6a	$S(r)_{\text{avg}}, S^c(r)_{\text{avg}}, S^l(r)_{\text{avg}}, \text{PCV}$
6b	$S(r)_{\text{proj}}, S^c(r)_{\text{proj}}, S^l(r)_{\text{proj}}, \text{PCV}$
6c	$S(r)_{\text{avg}}, S^c(r)_{\text{avg}}, S^l(r)_{\text{avg}}, S(r)_{\text{proj}}, S^c(r)_{\text{proj}}, S^l(r)_{\text{proj}}, \text{PCV}$

TABLE II. The integrated mean squared error between the reference and final reconstruction's two-point correlation functions. The error is very small, indicating that the simulated annealing algorithm was successful in perturbing the reconstructed assembly to fit the reference assembly's TPCFs.

Assembly reconstruction method	$\langle(\text{TPCF}_{\text{ref}} - \text{TPCF}_{\text{recon}})^2\rangle \times 10^{-6}$								
	1	2	3	4a	4b	5	6a	6b	6c
Isotropic spheres	1.02	1.60	0.87	1.30	–	1.36	1.64	–	–
Isotropic ellipsoids	0.97	1.82	0.87	2.18	–	1.47	1.34	–	–
Anisotropic ellipsoids	1.00	1.57	0.89	0.86	1.52	1.65	1.82	1.50	1.42

a given reconstruction method has accurately described the spatial relationships of the reference assembly.

A. Tortuosity

The tortuosity, τ , of a path is the ratio of the actual path length between two points over the shortest distance between these points. In a two-phase network containing multiple paths, tortuosity can be determined using a random walker algorithm. A random-walker particle is placed in a given phase of a multiphase assembly, taking discrete unit steps in random directions while staying within that phase [Fig. 3(a)]. Periodic boundary conditions are applied at the assembly's boundaries; reflective boundary conditions at the two-phase interface keep the random walkers within the percolating cluster [13]. In an unbounded phase, the mean-squared total distance traveled, $\langle R^2 \rangle$, by a set of random walkers is equal to the number of steps taken [Fig. 3(b)]. Reductions in $\langle R^2 \rangle$

reflect increasing tortuosities of the bounded phase geometry, where $\tau = \text{slope}_{\text{empty}}/\text{slope}_{\text{assembly}}$ [28].

Here, the tortuosity of the percolating pore space is calculated from the average trajectories of 1000 random walkers, where starting positions of the walkers are chosen randomly within the phase of interest. Each random walker takes a step of 1 voxel length, forward or backward, along any one of the three axes. The number of steps taken for each assembly varies to ensure the tortuosity calculations are based on a large enough sampling volume, as determined by the following process: (i) The random walker algorithm begins with each of the 1000 walkers taking 140 000 steps or iterations. This is repeated five times at 140 000 iterations, resulting in five tortuosity, τ , values (each time the algorithm is run, the random walkers' starting positions are randomly chosen). (ii) The number of iterations is then increased by 20 000 and rerun an additional five times. (iii) The median tortuosities obtained for both numbers of iterations are then compared. If the percentage point difference is $>10\%$, then an additional 20 000 steps are taken during the random walker algorithm, resulting in five more tortuosity values and a corresponding median. (iv) Steps (ii) and (iii) are repeated until the percentage point difference between two sequential median tortuosities is $<10\%$.

B. Percolating cluster volume

Previous studies have reported that TPCFs are sufficient for accurate assembly reconstructions [10–12]. However, in our experience, a TPCF alone, or in combination with other TPCFs, is typically insufficient to reproduce the cluster size distribution of the given reference assembly (see Secs. IV and V). Consequently, the percolating cluster volume (PCV) is added to the reconstruction process to produce a more accurate percolating cluster volume. Somewhat different in character than the TPCFs, the PCV is determined in the reference assemblies by identifying the volume of inclusion clusters that span the unit box space in the z direction. The PCV is used in the simulated annealing algorithm for select assembly reconstructions. When the PCV is not used in the reconstruction process, it can be used as an independent parameter to assess the accuracy of a given reconstruction.

C. Permeability

As discussed in the Introduction, permeability is a necessary but insufficient indicator of an accurate assembly reconstruction, as it integrates multiple geometric phase relationship characteristics. Thus, permeability should be similar in the

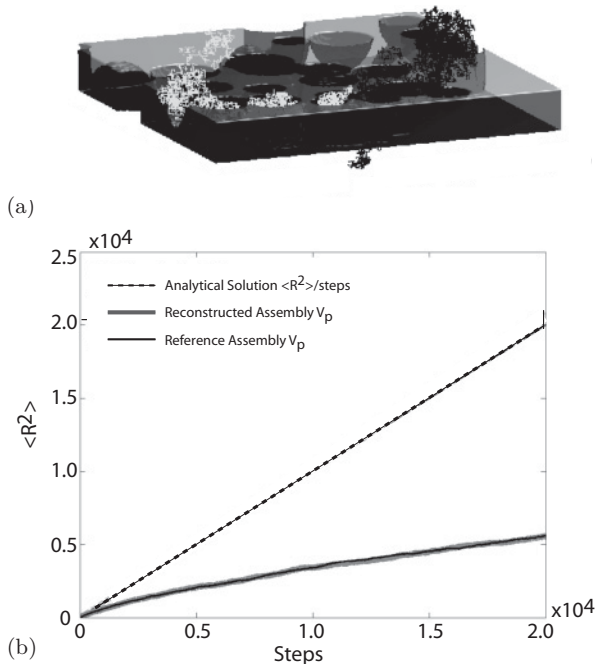


FIG. 3. (a) Examples of random walks through a percolating cluster. A three-dimensional slice of the percolating cluster is shown to demonstrate the movement of two random walkers (gray and black) within the inclusions. (b) Mean-squared displacement for 20 000 steps and 1000 random walkers.

reference and reconstructed assembly if the reconstruction is statistically accurate. However, it is unlikely permeability will be identical between the reference and reconstruction as fluid-flow bottlenecks or openings in the connected inclusion apertures could be present in specific instances of the reconstruction that are absent in the reference assembly (or vice versa). Furthermore, permeability can depend strongly on minute variations in microstructure (e.g., Refs. [16,17,29,30]). Thus, it is important to conduct several reconstructions for each of the composite reference assemblies and to base the composite reference assembly on multiple instances, as described in Sec. III.

The permeability of the reference and reconstructed assemblies are determined using numerical lattice-Boltzmann simulations of fluid flow [31–33]. Comprehensive overviews of the lattice-Boltzmann method can be found in Refs. [34–36]. This method can also be applied to a realistic porous medium that has been numerically characterized using high-resolution, three-dimensional microtomography. Detailed descriptions and comparisons with analytical solutions (where available) of the lattice-Boltzmann program used in this article are given in Refs. [37–40]. General experimental verification of three-dimensional lattice-Boltzmann simulations can be found in Refs. [41–43]. The particular lattice-Boltzmann model employed in this article is an incompressible single relaxation D3Q19 model with a collision frequency of 1 (i.e., a kinematic viscosity of $1/6 \Delta x^2/\Delta t$) [36].

The permeabilities of the synthetic assemblies are found using Darcy’s law [44]

$$k = -\frac{q\mu L}{\Delta P}, \quad (14)$$

where k is the viscous (Darcian) permeability, q is the volumetric fluid flow rate or flux per cross sectional area of the sample orthogonal to the fluid flow direction (determined by integrating the fluid flow vectors exiting the assembly over the surface area of the assembly’s face), μ is the dynamic viscosity of the test fluid passing through the porous medium, and ΔP is the change in fluid pressure across the sample length, L . We assume the synthetic test fluid is incompressible and apply a low pressure gradient to ensure laminar flow, allowing us to use the standard form of Darcy’s law given above [45,46].

IV. DISCUSSION

The three assembly types used in the reconstruction process are chosen to investigate how different reconstruction methods preserve the statistical relationships between the assemblies’ inclusions. We examine an isotropic spheroidal, isotropic ellipsoidal, and anisotropic ellipsoidal assembly, where the anisotropic assembly’s inclusions are preferentially aligned along the z axis.

Visual comparison between the reference and reconstructed assemblies is an unreliable method for determining the accuracy of the statistical reconstruction and provides no quantitative insights into how well macroscopic material properties have been reproduced. When determining if a statistical reconstruction of an assembly has been correctly performed, it is important to distinguish between reconstruction-dependent and -independent parameters of the given assembly. If an

accurate reconstruction has been accomplished, the resultant macroscopic material properties produced by the simulated annealing process should be very similar to those of the reference assembly, due to the TPCFs capturing the spatial relationships of the inclusions. Thus, independent parameters must be used to verify the accuracy of a reconstruction, as discussed in Sec. II. In this case, we have chosen to compare the pore fraction of the whole assembly and the pore fraction of the percolating cluster volume, in addition to the specific surface area, permeability and tortuosity of the percolating cluster volume. Figure 4 provides an overview of the reconstruction methods’ performances. An assessment of the reconstruction methods follows.

In general, Methods 1 and 2 (Table I), using a single TPCF, resulted in poorly reconstructed physical characteristics of the reference assembly (Fig. 4). This supports the findings in Ref. [11], where the authors assert multiple correlation functions should be used to optimize the accuracy of the reconstructions. However, in Method 3, followed after Refs. [12,15], we use $S(r)$ and $S^l(r)$ together with equally poor results. It is only when we add clustering information through the PCV or the $S^c(r)$ to the reconstruction algorithm that more consistently robust reconstructions are achieved. Furthermore, there appears to be a correlation between the pore fraction of the percolating cluster volume, ϕ_{PCV} , and the specific surface area of the percolating cluster, s_{PCV} . As the total specific surface area of a reference assembly is easily determined [Eq. (2)] and used during the reconstruction process (Sec. II), we initially assumed that the s_{PCV} would be trivial to reproduce in the reconstructed assemblies. However, the reconstructed assembly’s s_{PCV} is only accurately reproduced when the PCV or $S^c(r)$ is also used in the reconstruction process, indicating that cluster information is required to reconstruct an assembly’s s_{PCV} . This finding for continuous objects corroborates those of Ref. [27], where they determined a clustering function significantly improves the accuracy of a reconstructed, discretized assembly.

While we anticipated challenges in reconstructing anisotropic media, we did not anticipate difficulties in consistently reconstructing the more sensitive properties, such as permeability, in the isotropic media. However, there does not appear to be a relationship between our ability to reconstruct the ϕ_{PCV} and permeability, k , as we do not see a poorly reproduced permeability value corresponding to a poor PCV fit (Fig. 4). Conversely, a well reconstructed PCV does not necessarily result in a well-reconstructed permeability. Therefore, our inability to reconstruct an accurate k for any reconstruction method indicates permeability is a very sensitive physical property that can be significantly altered by a single small or large aperture between two inclusions of the same phase (e.g., Refs. [16,17,29,30]), particularly near the percolation threshold. Either of these situations can greatly restrict or increase flow through these regions, significantly altering the macroscale permeability of the assembly. An impermeable assembly could even result if a critical bottleneck of a percolating cluster is blocked. Therefore, a perfect permeability match between the reference and reconstructed assemblies was not anticipated, considering our limited sample size of 10 reconstructions for each method. Furthermore, as permeability, k , and tortuosity, τ , are related, it is difficult

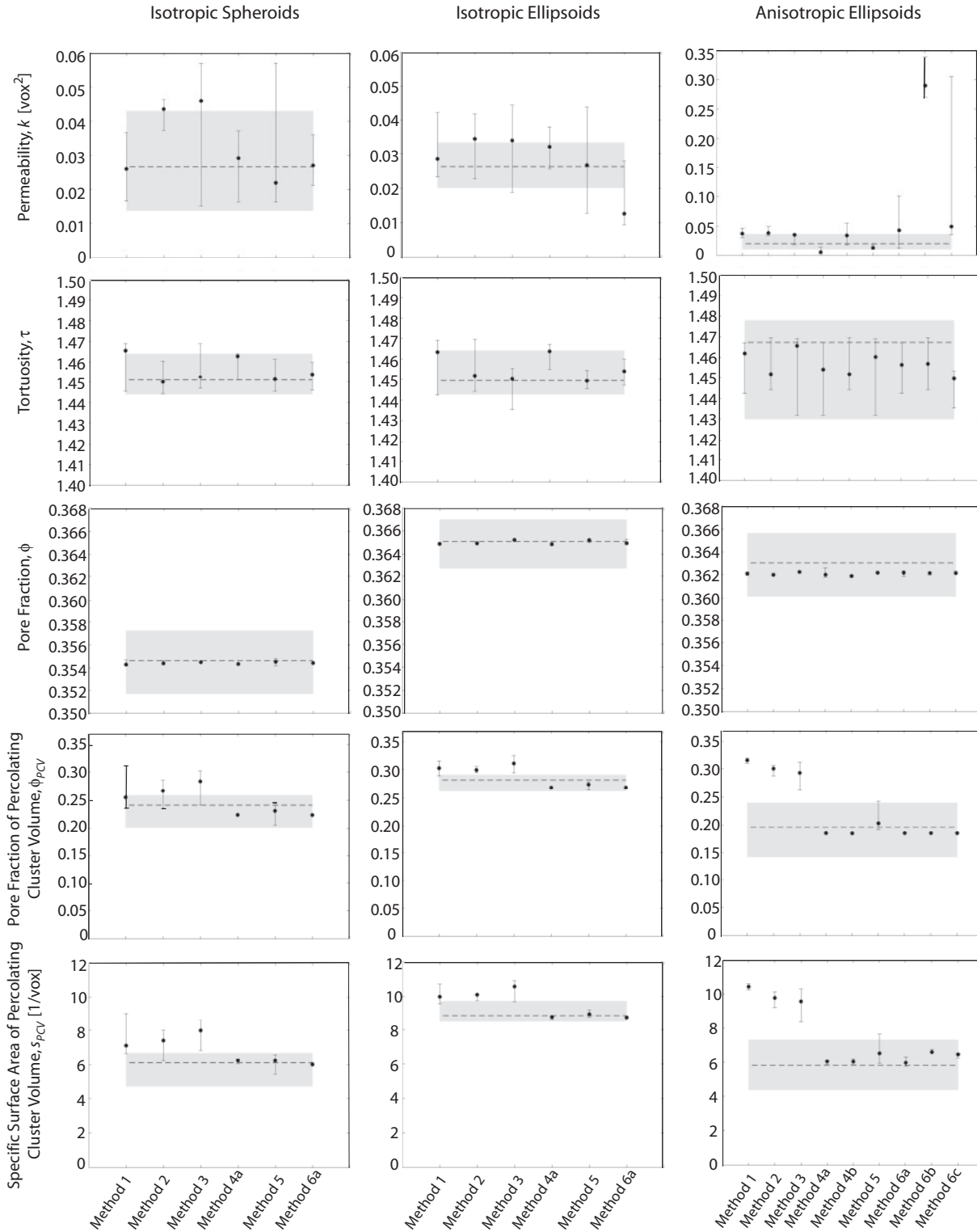


FIG. 4. Comparison of physical characteristics in reconstructed assemblies to those of the reference assemblies. The black circles are the median value of the 10 reconstruction assemblies, while the range of reconstruction values (vertical lines) shows the upper and lower quartile values of all the assemblies. The gray-shaded area represents the range between the upper and lower quartile values of the reference assembly, while the dashed line indicates the median value of the reference assembly. The reference assemblies are based on the combination of 10 instances of assemblies to reduce any anomalies that can appear in only one reference assembly.

to reconstruct an accurate k without an accurate τ . However, Fig. 4 shows a consistently reasonable result for τ , despite the accuracy variations in the reconstructed permeability.

The total pore fraction for a given TPCF is defined as the median of the y-axis intercepts from that correlation function's projections in the x , y , and z directions [Fig. 2(b)]. For the

isotropic assemblies, the pore fraction (or y intercept) is typically the same in each of the three dimensions. However, for the anisotropic assemblies, the pore fraction, ϕ , will be slightly different in the dimension of anisotropy (in this case, the z direction). Therefore, when the pore fraction's median value is calculated for a given correlation function, the function sampled along the direction of anisotropy can raise or lower the median ϕ . However, in this case, the difference between the ϕ of the reference and reconstructed assemblies is less than 10% (Fig. 4). Furthermore, the reconstructions of the anisotropic assemblies consistently reproduce ϕ between the upper and lower quartile of the reference assembly.

V. CONCLUSION

Beginning with what we perceive as the simplest geometric assembly to reconstruct, the isotropic spheroids, we found of all methods investigated (Table I), Methods 4a [$S(r)_{\text{avg}}$, $S^l(r)_{\text{avg}}$, and PCV] and 6a [$S(r)_{\text{avg}}$, $S^c(r)_{\text{avg}}$, $S^l(r)_{\text{avg}}$, and PCV] to be the most effective (Fig. 4). Method 5 [$S(r)_{\text{avg}}$, $S^c(r)_{\text{avg}}$, $S^l(r)_{\text{avg}}$] also reconstructed the assemblies well but failed to satisfactorily reproduce permeability. Therefore, we suggest Method 4a provides a close to optimal reconstruction method for isotropic spheroidal assemblies, as it produces excellent reconstructions, while the reconstruction process is less complicated than that of Method 6a.

None of the reconstruction methods effectively reproduce permeability for the isotropic ellipsoidal assemblies as well as initially anticipated. However, Methods 5 and 6a result in excellent reconstructions of the other physical characteristics, and Method 5 reproduced permeability satisfactorily.

Finally, reconstructing the permeability of the anisotropic assemblies proved difficult, likely due to the inherent sensitivity of the property, as discussed in Sec. IV. However, with a significantly larger assembly sample size, the overall sensitivity of the permeability property to the details of the microstructure would likely be reduced. The reconstruction results for the anisotropic ellipsoids show Methods 6a, 6b, and 6c producing good reconstructions, excluding the permeability. Furthermore, Methods 4a and 4b also produce robust reconstructions, with permeability results for Method 4b proving slightly better than in Methods 4a and 6a, 6b, and 6c. However, Method 5 reproduces permeability the best but does not reproduce the specific surface area of the percolating cluster as well as Methods 4a and 4b and 6a, 6b, and 6c, and Method 6a produces a permeability that overlaps with the reference permeability. Due to the difficulty of statistically reproducing anisotropic geometries, the reader should choose a reconstruction method while keeping in mind each method's strengths and weaknesses.

The purpose of this research is to determine the optimal method to reconstruct a two-phase medium, while preserving its macroscopic material properties. The spatial correlation functions from an accurate reconstruction can also be applied to an upscaling method, where the physical properties of a representative elementary volume can be examined. We focus on reconstructing continuous microstructures, as opposed to discrete assemblies visualized as voxels (3D) or pixels (2D). We conclude that the original findings of Yeong and Torquato [12,15], with the small addition of the percolating

cluster volume, PCV, or two-point cluster function, $S^c(r)$, to the reconstruction process, prove to satisfactorily reconstruct 2D and 3D isotropic two-phase media. However, anisotropic media are more difficult to reconstruct, as the dimension that reflects the anisotropy has significantly different physical characteristics than the other two dimensions. Therefore, we find the optimal reconstruction method to capture a medium's anisotropy should include the PCV and/or $S^c(r)$, with the possibility of including projected two-point correlation functions.

ACKNOWLEDGMENTS

The authors acknowledge support by the National Science Foundation (NSF) under Grant No. EAR-0510723 and Grant No. DMS-0724560. M.O.S. also thanks the George and Orpha Gibson endowment for its generous support of the Hydrogeology and Geofluids group. We would also like to thank the anonymous reviewers for their insightful comments that improved the manuscript.

APPENDIX

In contrast to previous studies, which calculated two-point correlation functions based on digitized images of the underlying microstructure, this study calculates two-point correlation functions from a continuum description of an assembly. The assembly is composed of collections of individual inclusions (e.g., spheres and ellipsoids). However, this method can also be used with digitized images, such as voxelized data. In this section, we describe the methods used to calculate the two-point correlation functions, $S(r)$, $S^l(r)$, and $S^c(r)$, in addition to the percolating cluster volume, PCV, for these assemblies.

Consider an assembly of inclusions, Λ , comprising N^c clusters, Λ_n^c , such that $\Lambda = \{\Lambda_n^c : 1 \leq n \leq N^c\}$. Given a line segment, l_i , from \mathbf{x}^a to \mathbf{x}^b , a function $f(l_i, t)$ is introduced for $0 \leq t \leq 1$, where

$$f(l_i, t) = \begin{cases} 0 & \text{if } \mathbf{x}^a + t(\mathbf{x}^b - \mathbf{x}^a) \notin \Lambda \\ 1 & \text{if } \mathbf{x}^a + t(\mathbf{x}^b - \mathbf{x}^a) \in \Lambda \end{cases}, \quad (\text{A1})$$

i.e., the function is zero if the point on the line, a proportion t along its total length, is outside the inclusion and equal to 1 if the point is inside the inclusion.

In practice, $f(l_i, t)$ is not calculated directly. Instead, for each line segment under consideration, we determine if the end points are within the assembly, and record points along the lines that intersect the inclusions in the assemblies. From this information, it is a relatively simple matter to recover $f(l_i, t)$ for any value of t .

The probability that two random points separated by r on a line segment of length $l_i > r$ are both contained within the assembly is

$$s_i(r) = \frac{1}{1 - r/l_i} \int_0^{1-r/l_i} f(l_i, t) f(l_i, t + r/l_i) dt. \quad (\text{A2})$$

Given a sufficiently large number of line segments, the two-point probability function $S(r)$ is approximated by

$$S(r) \approx \sum_{l_i > r} s_i(r) [l_i - r] / \sum_{l_i > r} [l_i - r]. \quad (\text{A3})$$

The two-point cluster and line path functions are calculated in a similar manner by introducing two new functions, $f_n^c(l, t)$ and $f_n^{ch}(l, t)$:

$$f_n^c(l, t) = \begin{cases} 1 & \text{if } x^a + t(x^b - x^a) \text{ is in the } n\text{th cluster} \\ 0 & \text{otherwise} \end{cases} \quad (\text{A4})$$

and

$$f_n^{ch}(l_i, l, t) = \begin{cases} 1 & \text{if } x^a + t(x^b - x^a) \text{ is in the } n\text{th chord} \\ 0 & \text{otherwise} \end{cases}. \quad (\text{A5})$$

For our purposes, a chord is defined as a line joining two points on the edge of a cluster that lies entirely within the cluster.

The probability that two random points separated by r on l_i are both contained within the same cluster is

$$s_i^c(r) = \frac{1}{1 - r/l_i} \sum_{n=1}^{N^c} \int_0^{1-r/l_i} f_n^c(l_i, t) f_n^c(l_i, t + r/l_i) dt, \quad (\text{A6})$$

while the probability that the line between those two points is completely covered is

$$s_i^l(r) = \frac{1}{1 - r/l_i} \sum_{n=1}^{N^{ch}} \int_0^{1-r/l_i} f_n^{ch}(l_i, t) f_n^{ch}(l_i, t + r/l_i) dt. \quad (\text{A7})$$

With a sufficiently large number of line segments, $S^c(r)$ and $S^l(r)$ are approximated by

$$S^c(r) \approx \sum_{l_i > r} s_i^c(r) [l_i - r] / \sum_{l_i > r} [l_i - r] \quad (\text{A8})$$

and

$$S^l(r) \approx \sum_{l_i > r} s_i^l(r) [l_i - r] / \sum_{l_i > r} [l_i - r], \quad (\text{A9})$$

respectively.

The two-point correlation functions given above describe probabilities for randomly aligned line segments. For a given orientation, \mathbf{n} , the probability density distribution functions are calculated from

$$S^X(r, \mathbf{n}) \approx \sum_{l_i > r} s_i^X(r, \mathbf{n}) [l_i - r] / \sum_{l_i > r} [l_i - r], \quad (\text{A10})$$

where $S^X(r, \mathbf{n}) \in \{S(r, \mathbf{n}), S^c(r, \mathbf{n}), S^l(r, \mathbf{n})\}$ are the two-point probability functions and $s^X(r, \mathbf{n}) \in \{s(r, \mathbf{n}), s^c(r, \mathbf{n}), s^l(r, \mathbf{n})\}$ are the associated line segment probabilities for the orientation, \mathbf{n} .

The cluster volume distribution function is calculated from the same data used in the two-point cluster function, $S^c(r)$. To calculate the two-point cluster function, each connected cluster of objects within the assembly must be found and each chord identified with the cluster that contains it. The volume of the n th cluster V_n^c can be calculated from this information via

$$V_n^c = V^T \sum_i \left[l_i \int_0^1 f_n^c(l_i, t) dt \right] / \sum_j l_j, \quad (\text{A11})$$

where V^T is the total assembly volume. The percolating cluster volume is the sum of the volumes of the space-spanning cluster(s) in a given assembly.

-
- [1] J. Høst-Madsen and K. Høgh Jensen, *J. Hydrol.* **135**, 13 (1992).
[2] O. Melnik, *Bull. Volcanol.* **62**, 153 (2000).
[3] N. Koshiba, J. Ando, X. Chen, and T. Hisada, *J. Biomech. Eng.* **129**, 374 (2007).
[4] O. Anwar Bég, R. Bhargava, S. Rawat, K. Halim, and H. S. Takhar, *Meccanica* **43**, 391 (2008).
[5] G. W. Scherer, *Mater. Struct.* **39**, 1041 (2006).
[6] A. M. Kraynik, *Annu. Rev. Fluid Mech.* **20**, 325 (1988).
[7] B. Moore, T. Jaglinski, D. Stone, and R. Lakes, *Cell. Polymer* **26**, 1 (2007).
[8] L. Nicolais, E. Drioli, and R. F. Landel, *Polymer* **14**, 21 (1973).
[9] A. I. Abdel-Hadi, O. I. Zhupanska, and N. D. Cristescu, *Mech. Mater.* **34**, 373 (2002).
[10] S. Torquato, *Annu. Rev. Mater. Res.* **32**, 77 (2002).
[11] S. Torquato and G. Stell, *J. Chem. Phys.* **77**, 2071 (1982).
[12] C. L. Y. Yeong and S. Torquato, *Phys. Rev. E* **57**, 495 (1998).
[13] K. Makrodimitris, G. K. Papadopoulos, C. Philippopoulos, and D. N. Theodorou, *J. Chem. Phys.* **117**, 5876 (2002).
[14] B. Lu and S. Torquato, *Phys. Rev.* **45**, 922 (1992).
[15] C. L. Y. Yeong and S. Torquato, *Phys. Rev. E* **58**, 224 (1998).
[16] M. O. Saar and M. Manga, *J. Geophys. Res.* **109**, B04204 (2004).
[17] S. D. C. Walsh and M. O. Saar, *J. Volcanol. Geotherm. Res.* **177**, 1011 (2008).
[18] D. L. Johnson, J. Koplik, and L. M. Schwartz, *Phys. Rev. Lett.* **57**, 2564 (1986).
[19] M. Avellaneda and S. Torquato, *Phys. Fluids A* **3**, 2529 (1991).
[20] J. G. Berryman and S. C. Blair, *J. Appl. Phys.* **62**, 2221 (1987).
[21] S. Torquato, J. D. Beasley, and Y. C. Chiew, *J. Chem. Phys.* **88**, 6540 (1988).
[22] N. Metropolis, A. W. Rosenbluth, M. N. Rosenbluth, A. H. Teller, and E. Teller, *J. Chem. Phys.* **21**, 1087 (1953).
[23] Y. Nourani and B. Andresen, *J. Phys. A: Math. Gen.* **31**, 8373 (1998).
[24] C. Klug and K. V. Cashman, *Bull. Volc.* **58**, 87 (1996).
[25] Y. Jiao, F. H. Stillinger, and S. Torquato, *Phys. Rev. E* **76**, 031110 (2007).
[26] Y. Jiao, F. H. Stillinger, and S. Torquato, *Phys. Rev. E* **77**, 031135 (2008).
[27] Y. Jiao, F. H. Stillinger, and S. Torquato, *Proc. Natl. Acad. Sci. USA* **106**, 17634 (2009).
[28] Y. Watanabe and Y. Nakashima, *Comput. Geosci.* **28**, 583 (2002).
[29] R. A. Freeze and J. A. Cherry, *Groundwater* (Prentice Hall, Upper Saddle River, NJ, 1979), pp. 73–75.
[30] M. O. Saar and M. Manga, *Geophys. Res. Lett.* **26**, 111 (1999).
[31] B. Ferréol and D. H. Rothman, *Transp. Porous Media* **20**, 3 (1995).
[32] F. M. Auzerais, J. Dunsmuir, B. Ferréol, N. Marty, J. F. Olsen, T. S. Ramakrishnan, D. H. Rothman, and L. M. Schwartz, *Geophys. Res. Lett.* **23**, 705 (1996).

- [33] C. Pan, L.-S. Luo, and C. T. Miller, *Comput. Fluid.* **35**, 898 (2006).
- [34] D. H. Rothman and S. Zaleski, *Lattice Gas Cellular Automata: Simple Models of Complex Hydrodynamics* (Cambridge University Press, Cambridge, UK, 1997).
- [35] D. A. Wolf-Gladrow, *Lattice-Gas Cellular Automata and Lattice Boltzmann Models* (Springer, Berlin, 2000).
- [36] S. Succi, *The Lattice Boltzmann Equation for Fluid Dynamics and Beyond* (Oxford University Press, Oxford, 2001).
- [37] S. D. C. Walsh, M. O. Saar, P. Bailey, and D. J. Lilja, *Comput. Geosci.* **35**, 2353 (2009).
- [38] J. Myre, S. D. C. Walsh, D. Lilja, and M. O. Saar, *Concurrency Comput. Pract. Ex.* (2010).
- [39] S. D. C. Walsh and M. O. Saar, *Water Resour. Res.* **46**, W07517 (2010).
- [40] S. D. C. Walsh and M. O. Saar, *Phys. Rev. E* **82**, 066703 (2010).
- [41] B. Manz, L. F. Gladden, and P. B. Warren, *AIChE J.* **45**, 1845 (1999).
- [42] M. D. Mantle, B. Bijeljic, A. J. Sederman, and L. F. Gladden, *Magn. Reson. Imaging* **19**, 527 (2001).
- [43] M. D. Mantle, A. J. Sederman, and L. F. Gladden, *Chem. Eng. Sci.* **56**, 523 (2001).
- [44] H. Darcy, *Les Fontaines Publiques de la Ville de Dijon* (Dalmont, Paris, 1856).
- [45] O. Reynolds, *Papers on Mechanical and Physical Subjects* (Cambridge University Press, Cambridge, UK, 1900), Vol. II.
- [46] P. Forchheimer, *Z. Ver. Dtsch. Ing.* **45**, 1781 (1901).